EBioMedicine 54 (2020) 102723

Contents lists available at ScienceDirect

EBioMedicine

journal homepage: www.elsevier.com/locate/ebiom

Research paper

Identification, clinical manifestation and structural mechanisms of mutations in AMPK associated cardiac glycogen storage disease

Dan Hu[a,b,1,*], Dong Hu[c,1], Liwen Liu[d,1], Daniel Barr[e], Yang Liu[f], Norma Balderrabano-Saucedo[g], Bo Wang[d], Feng Zhu[h,i], Yumei Xue[f], Shulin Wu[f], BaoLiang Song[j], Heather McManus[k], Katherine Murphy[e], Katherine Loes[e], Arnon Adler[l], Lorenzo Monserrat[m], Charles Antzelevitch[n,o], Michael H. Gollob[l], Perry M. Elliott[p], Hector Barajas-Martinez[n,o,1]

[a] Department of Cardiology and Cardiovascular Research Institute, Renmin Hospital of Wuhan University, 238 Jiefang Road, Wuhan 430060, China
[b] Hubei Key Laboratory of Cardiology, Wuhan 430060, China
[c] Center for Stem Cell Research and Application, Union Hospital, Tongji Medical College, Huazhong University of Science and Technology, Wuhan, China
[d] Department of Ultrasound, Xijing Hospital, Fourth Military Medical University, Xi'an, China
[e] Department of Chemistry, University of Mary, 7500 University Drive, Bismarck, ND, USA
[f] Guangdong Cardiovascular Institute, Guangdong General Hospital, Guangdong Academy of Medical Sciences, 106 Zhongshan Er Road, Guangzhou 510080, China
[g] Department of Cardiology, Children Hospital of Mexico Federico Gómez, México, D.F., México
[h] Clinic Center of Human Gene Research, Union Hospital, Tongji Medical College, Huazhong University of Science and Technology, China
[i] Department of Cardiology, Union Hospital, Tongji Medical College, Huazhong University of Science and Technology, China
[j] College of Life Sciences, Wuhan University, Wuhan, China
[k] Department of Chemistry and Biochemistry, Utica College, Utica, NY, USA
[l] Department of Physiology and the Peter Munk Cardiovascular Molecular Medicine Laboratory, Toronto General Hospital, University of Toronto, Toronto, ON, Canada
[m] Health in Code SL, A Coruña, Spain
[n] Lankenau Institute for Medical Research, Wynnewood, PA, USA
[o] Lankenau Heart Institute, Sidney Kimmel College of Medicine, Thomas Jefferson University, USA
[p] University College London and St. Bartholomew's Hospital, London, United Kingdom

ARTICLE INFO

Article History:
Received 11 September 2019
Revised 8 February 2020
Accepted 3 March 2020
Available online xxx

Keywords:
Genetics
Arrhythmia
PRKAG2 syndrome
Cardiomyopathy
Heart failure
Sudden cardiac death

ABSTRACT

Background: Although 21 causative mutations have been associated with *PRKAG2* syndrome, our understanding of the syndrome remains incomplete. The aim of this project is to further investigate its unique genetic background, clinical manifestations, and underlying structural changes.
Methods: We recruited 885 hypertrophic cardiomyopathy (HCM) probands and their families internationally. Targeted next-generation sequencing of sudden cardiac death (SCD) genes was performed. The role of the identified variants was assessed using histological techniques and computational modeling.
Findings: Twelve *PRKAG2* syndrome kindreds harboring 5 distinct variants were identified. The clinical penetrance of 25 carriers was 100.0%. Twenty-two family members died of SCD or heart failure (HF). All probands developed bradycardia (HRmin, 36.3 ± 9.8 bpm) and cardiac conduction defects, and 33% had evidence of atrial fibrillation/paroxysmal supraventricular tachycardia (PSVT) and 67% had ventricular preexcitation, respectively. Some carriers presented with apical hypertrophy, hypertension, hyperlipidemia, and renal insufficiency. Histological study revealed reduced AMPK activity and major cardiac channels in the heart tissue with K485E mutation. Computational modelling suggests that K485E disrupts the salt bridge connecting the β and γ subunits of AMPK, R302Q/P decreases the binding affinity for ATP, T400N and H401D alter the orientation of H383 and R531 residues, thus altering nucleotide binding, and N488I and L341S lead to structural instability in the Bateman domain, which disrupts the intramolecular regulation.

Abbreviation: AMPK, AMP-activated protein kinase; AMPK-α-pThr172, α AMPK Thr172 phosphorylation; CBS, Cystathionine beta-synthase; DAPI, Diamidino-2-phenylindole; EMB, Endomyocardial biopsy; EVS, Exome Variant Server; ExAC, Exome Aggregation Consortium; HCM, Hypertrophic cardiomyopathy; HF, Heart failure; HGMD, Human Gene Mutation Database; HMGCR, 3-Hydroxy-3-Methylglutaryl-CoA Reductase; LV, Left ventricle; LVH, Left ventricular hypertrophy; MAF, Minor Allele Frequency; RMSF, Root mean square fluctuations; PBS, Phosphate-buffered saline; PSVT, Paroxysmal supraventricular tachycardia; RMSD, Root mean squared displacement; SBS, Subunit binding sequence; SCD, Sudden cardiac death

* Corresponding author at: Department of Cardiology and Cardiovascular Research Institute, Renmin Hospital of Wuhan University, 238 Jiefang Road, Wuhan 430060, China.
E-mail addresses: rm002646@whu.edu.cn, hudan0716@hotmail.com (D. Hu).
[1] These authors contributed equally as first author.

https://doi.org/10.1016/j.ebiom.2020.102723

Interpretation: Including 4 families with 3 new mutations, we describe a cohort of 12 kindreds with *PRKAG2* syndrome with novel pathogenic mechanisms by computational modelling. Severe clinical cardiac phenotypes may be developed, including HF, requiring close follow-up.

1. Introduction

Unexplained left ventricular hypertrophy (LVH) is a common clinical observation and when excessive is usually attributed to hypertrophic cardiomyopathy (HCM), an autosomal dominant hereditary disease caused principally by mutations in genes encoding the sarcomeric proteins [1,2]. However, other disease-causing genes have also been identified, such as *PRKAG2*, which encodes the AMP-activated protein kinase (AMPK) γ2 subunit [3]. Defects in *PRKAG2* are associated with a cardiac syndrome consisting of familial ventricular preexcitation, conduction defect, bradycardia, cardiac hypertrophy mimicking HCM, and atrial tachyarrhythmia [3,4]. Histological studies of myocardial tissue from affected individuals, transgenic mice models [5–7] and stem cell models [7–9] expressing mutant forms of *PRKAG2* confirmed glycogen storage defects and also broad implications in cell growth as the pathologic basis of mutation. Unlike HCM, individuals with *PRKAG2* mutations have a higher incidence of progressive cardiac conduction disease requiring implantation of a pacemaker. It is therefore important to distinguish the phenocopy condition of hypertrophy associated with *PRKAG2* mutations from those due to sarcomere protein defects. The objective of the present study is to further delineate the unique genetic background and clinical perspective of *PRKAG2* syndrome, together with less commonly described extracardiac features, prognosis, and management. We also highlight mechanistic insights derived through the evaluation of identified mutations using computer models.

2. Materials and methods

See additional details in Supplementary Materials.

2.1. Clinical study protocol

Overall, 885 patients with HCM, defined as unexplained increased left ventricle (LV) wall thickness ≥13 mm in one or more LV myocardial segments by any cardiac imaging technique, were retrospectively enrolled internationally from 2013 to 2018 [2]. Among them, we gathered the detailed clinical data from the patients diagnosed with disease-causing mutations of *PRKAG2*. This study was approved by each Hospital Institutional Review Board and performed in accordance with the declaration of Helsinki. The participants gave written informed consent. Additional clinical description of the patients is available in the supplementary materials.

2.2. Genetic testing

Genomic DNA was extracted from peripheral blood leukocytes for all probands and available family members, then screened by next generation sequencing of targeted genes for SCD . The panel was designed using the tool Array (Agilent Technologies, Inc.), including all isoforms described by UCSC. The full list of target genes is provided in supplementary Table 1. Identified genetic variations were consulted in the Human Gene Mutation Database (HGMD). The possible pathogenicity of the alteration was consulted *in silico* using Polyphen, SIFT, and PROVEAN. Allelic frequency was compared to genetic variations in healthy populations in the Exome Variant Server (EVS), the dbSNP database, the Exome Aggregation Consortium (ExAC

Research in context

Evidence before this study

Recent study shows defects in *PRKAG2* are associated with a cardiac syndrome tetrad consisting of familial ventricular preexcitation, conduction system disease and cardiac hypertrophy mimicking HCM, as well as atrial tachyarrhythmia. Histological studies of myocardial tissue from affected individuals, transgenic mice expressing mutant forms and stem cell model of the *PRKAG2* gene confirmed glycogen storage and also broad implications in cell growth as the pathologic basis for this cardiac syndrome. It is therefore important to distinguish hypertrophy associated with *PRKAG2* mutations from that due to sarcomere protein defects. Our previous study revealed K485E mutant could disrupt a salt bridge with the conserved D248 residue in the AMPK $\boldsymbol{\beta}$ subunit, and promote severe prognosis. The objective of the present study is to further delineate the unique genetic background, mechanistic insights, and clinical perspective of the *PRKAG2* cardiac syndrome, together with less commonly described extracardiac features, prognosis, and management.

Added value of this study

With the unmasking of a large cohort of probands with *PRKAG2* cardiac syndrome among 885 international subjects with HCM, both the numbers of carriers and mutations are increased substantially. The clinical penetrance of 25 carriers was 100.0% and 21 extra family members died of sudden cardiac death or heart failure. The *PRKAG2* heart specimen with K485E developed end-stage HF with 1043 g, as well as reduced AMPK activity and major cardiac channels in the heart tissue. This study is the first to describe evidence of apical hypertrophy and severe kidney injury in *PRKAG2* cardiac syndrome patients. Computational modeling predicted K485E disrupted a salt bridge, R302Q/P decreases the binding affinity for ATP, T400N and H401D alter the orientation of H383 and R531, and both N488I and L341S lead to structural instability. Transfer entropy analysis revealed a pathway of communication between the CBS and catalytic domains, by which R302, H401, and L341 relay information via the K485/D248 salt bridge through $\boldsymbol{\beta}$ to $\boldsymbol{\alpha}$ subunit. This investigation and future studies hold promise not only to seeking specific therapeutics for *PRKAG2* syndrome, but more broadly to understanding the cellular energy sensor and the potential target to treat more prevalent metabolic and cardiac diseases.

Implications of all the available evidence

Computational modelling implicates novel pathogenic mechanisms of disease pathogenesis in various mutations, which maybe the potential target to treat more prevalent metabolic and cardiac diseases. Including 4 families with 3 new mutations, we describe a cohort of 12 kindreds with *PRKAG2* syndrome. Severe clinical cardiac phenotypes may be developed, including HF, which requires close follow-up and heart transplantation should be considered in time.

Browser), and the 1000 genomes database. In addition, alignment between different species was performed using the UNIPROT database to identify conservation of the region that included the genetic variation. We have ruled out those cases with any additional rare variation in other suspicious genes.

PRKAG2 mutations were confirmed by means of Sanger sequencing (RefSeq *PRKAG2:* NM_016203.3). The identification of known pathogenic variants was based on mutations reported to cause cardiovascular disease in the literature previously. Novel variants considered to be pathogenic were either: (1) stop/frameshift variants; (2) missense mutations positioned in the amino acid conservative region across species (Grantham score); (3) splice-site variations fulfilling the GT-AT rules; (4) predicted to be possibly damaging or disease-causing by the bioinformatic programs; and (5) uncommon (Minor Allele Frequency [MAF] $< 0.5\%$) from public database of healthy human variants, and co-segregated with the phenotype in the family.

2.3. Histology and AMPK activity analysis

The cardiac transplantation and biopsy for K485E carrier (proband 12) was performed in June 2014, and the biopsy for ventricular tissue of R302P carrier (proband 8) was performed in Oct 2017. Tissue samples, excised from three age and gender-matched patients with valvular heart diseases, were used as study controls. Genetic screening for *PRKAG2* mutation was negative in these 3 patients.

Sections were evaluated after staining with HE, Masson's trichrome, PAS, and Congo-Red staining using routine protocols. In addition, AMPK activity was estimated from α AMPK Thr172 phosphorylation (AMPK-α-pThr172).

2.4. Immunohistochemical analysis of ion-channel expression and distribution

Cardiac tissues were fixed with 4% paraformaldehyde and were permeated with 0.3% Triton X-100. After blocking with 10% donkey serum in phosphate-buffered saline (PBS) for 2 h, the coverslips with tissue sections were incubated at 4 °C with the various ionic antibodies diluted in PBS overnight. Then, the coverslips were exposed to secondary antibodies [Anti-CACNA1C antibody (ab84814), Anti-KCNA5 antibody (ab101788), Anti-KCNH2 antibody (ab81160), Anti-KCNQ1 antibody (ab84819), Anti-Kir2.1 antibody (ab65796), Anti-Kir6.2 antibody (ab79171), Anti-Kv4.3 antibody (ab99045), and Anti-Nav1.5 antibody (ab56240) from Abcam Inc; Anti-p-AMPKα1/2 (Thr 172) antibody (sc-33,524) from Santa Cruz Biotechnology Inc] and were rinsed three times with PBS. 4′,6-Diamidino-2-phenylindole (DAPI) is a fluorescent DNA dye to mark nucleus. Confocal microscopy analysis was carried out using Carl Zeiss LSM710 confocal system.

2.5. System preparation and electrostatic calculations

The coordinates of mammalian AMPK were obtained from the protein data bank. Mutants in the gamma subunit were built from the existing sidechains of the WT protein using the Mutate Residue plug-in for VMD. The Poisson-Boltzmann equation was solved analytically for both WT and mutant proteins. Dielectric constants of 1 and 78.54 were used for the solute and solvent, respectively.

2.6. Simulation protocol

All systems were solvated in a box of TIP3P water sized to extend a minimum of 10 Å beyond the protein non-hydrogen atoms. After minimization and heating, each system was equilibrated for 2 ns followed by 10 ns of production run. All simulations were performed using NAMD in the NPT ensemble at 1atm and 300 K using the CHARMM22 all-atom protein force field with the CMAP correction.

Transfer entropy provides a description of the information flow in a dynamic system, and has been used to elucidate pathways of communication. To assess the nature of long-range communication in AMPK, it was calculated using the dynamic Gaussian Network Model. Following Eq. 10 from reference [10], the sum of each row of the transfer entropy matrix was used to measure the entropic activity of each residue.

2.7. Statistical analysis

Data are presented as mean±SD of patient characteristics and mean±SEM of experimental data. Analyses of the root mean square fluctuations (RMSF) and radius of gyration were performed using Carma. A block analysis was performed to assess the convergence of RMSF of the CA atoms during the simulations. For statistical analysis, Student *t*-test and analysis of variance test were used to compare 2 and $\geq$3 groups separately (SPSS Inc., Chicago, IL). Differences were considered statistically significant at a value of $p < 0.05$.

3. Results

3.1. Clinical examination of probands and their families

Of 885 HCM cases evaluated internationally, we identified 12 independent families with *PRKAG2* syndrome (Figs. 1–3). Among 25 carriers, all genotype positive cases demonstrated clinical manifestations, defining the clinical penetrance rate as 100.0%. The average age of first symptom presentation was 22.0 ± 8.1y/o (IQR, 12.0), and 58.3% were male. Family history revealed 18 cases of SCD (61.1% males), and 4 deaths from heart failure (HF, all females), with the age for death of 30.5 ± 10.9y/o (IQR, 22y/o). Two male patients required heart transplantation. The uncle of Proband 9 underwent transplantation at 50y/o because of serious HF. Proband 12 also developed severe HF soon after publication of our previous study detailing K485E mutation [11]. Fortunately, as a result of accurate prediction and timely-adjusted clinical guidance, he received a cardiac transplant at 22y/o. One R302Q$^{+/-}$ carrier with HCM in family 4 (Patient II3 in Fig. 1d) died of HF nearly 30 years after the pacemaker was implanted. One patient underwent surgical myectomy at 25y/o and died due to post-surgical complications. Twelve cases (50%) received permanent device implantation. The probability of developing the hallmark clinical features in our probands of bradycardia and CCD was 100%. Paroxysmal atrial fibrillation / paroxysmal supraventricular tachycardia (PSVT), ventricular preexcitation, and SCD were observed in 33.3%, 66.7%, and 16.7% of probands, respectively. Their average of NYHA level, left ventricular EF, and thickest LV wall was III, 56.7%±13.5%, and 31.2 ± 7.2 mm.

Although most cases demonstrated typical asymmetrical, septal hypertrophy, we first discovered 2 cases with severe apical hypertrophy in *PRKAG2* syndrome (Proband 5 and 11). An endomyocardial biopsy (EMB) with HE staining of cardiac tissue from proband 8 confirmed cardiomyocyte hypertrophy, partial myocyte degeneration and nuclear enlargement, and congo-red staining suggested secondary amyloidosis (Fig. 3g). Proband 12 with K485E mutation finally developed end-stage HF with his heart mass of 1043 g (Fig. 4a-c, Supplementary Fig. 1). The phosphorylation level of the AMPK alpha subunit was measured by immunohistochemistry (Fig. 4d-i). The relative activity of AMPK was 0.46±0.03 in the control RA tissue, whereas it was significantly reduced in the patient's RA tissue (0.09±0.02, $P<0.01$, Fig. 4j). In accordance with other findings [12,13], pathological changes included marked hypertrophy of cardiomyocytes, myofibrillar disarray, interstitial fibrosis, intracellular vacuolization, and accumulation of large amounts of glycogen (Supplementary Figs. 2–3). As far as protein level, most potassium (Kv7.1, Kv11.1, Kv1.5, Kv4.3, Kir6.2, Kir2.1) and calcium channels (Cav1.2) have reduced expression with varying degrees (Supplementary Figs. 4–8), whereas there was no significant change in the patient's atrial

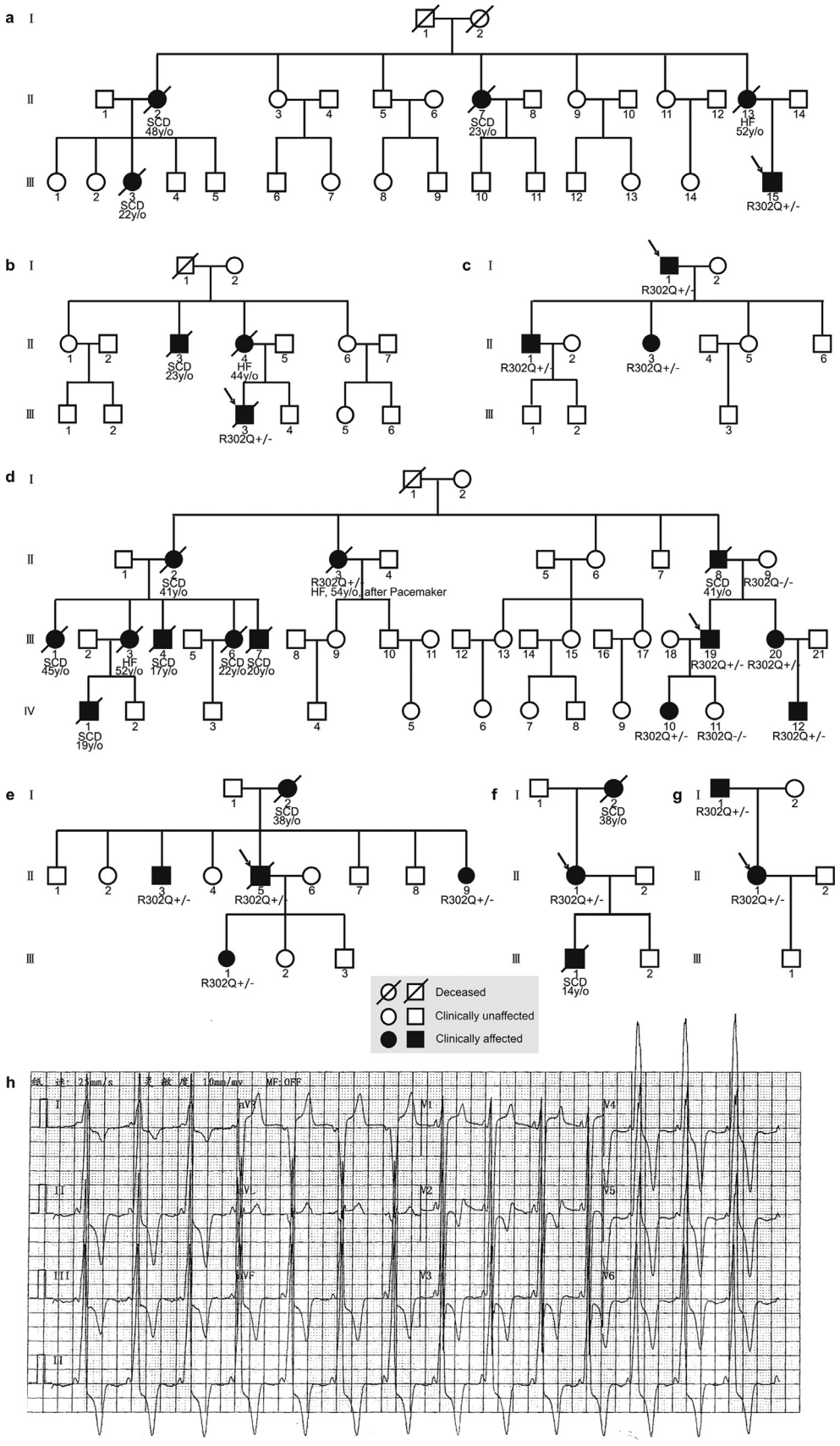

Fig. 1. Clinical records of R302Q mutant carriers. (**a-g**) Family pedigrees of Proband 1−7. +/- indicates a heterozygous mutation, circles/squares represent female/male subjects. The arrow indicates the proband. (**h**) ECG of Proband 2 (deceased) displaying preexcitation, complete left bundle branch block, left ventricular hypertrophy, PR interval 70 ms, and QRS 145 ms.

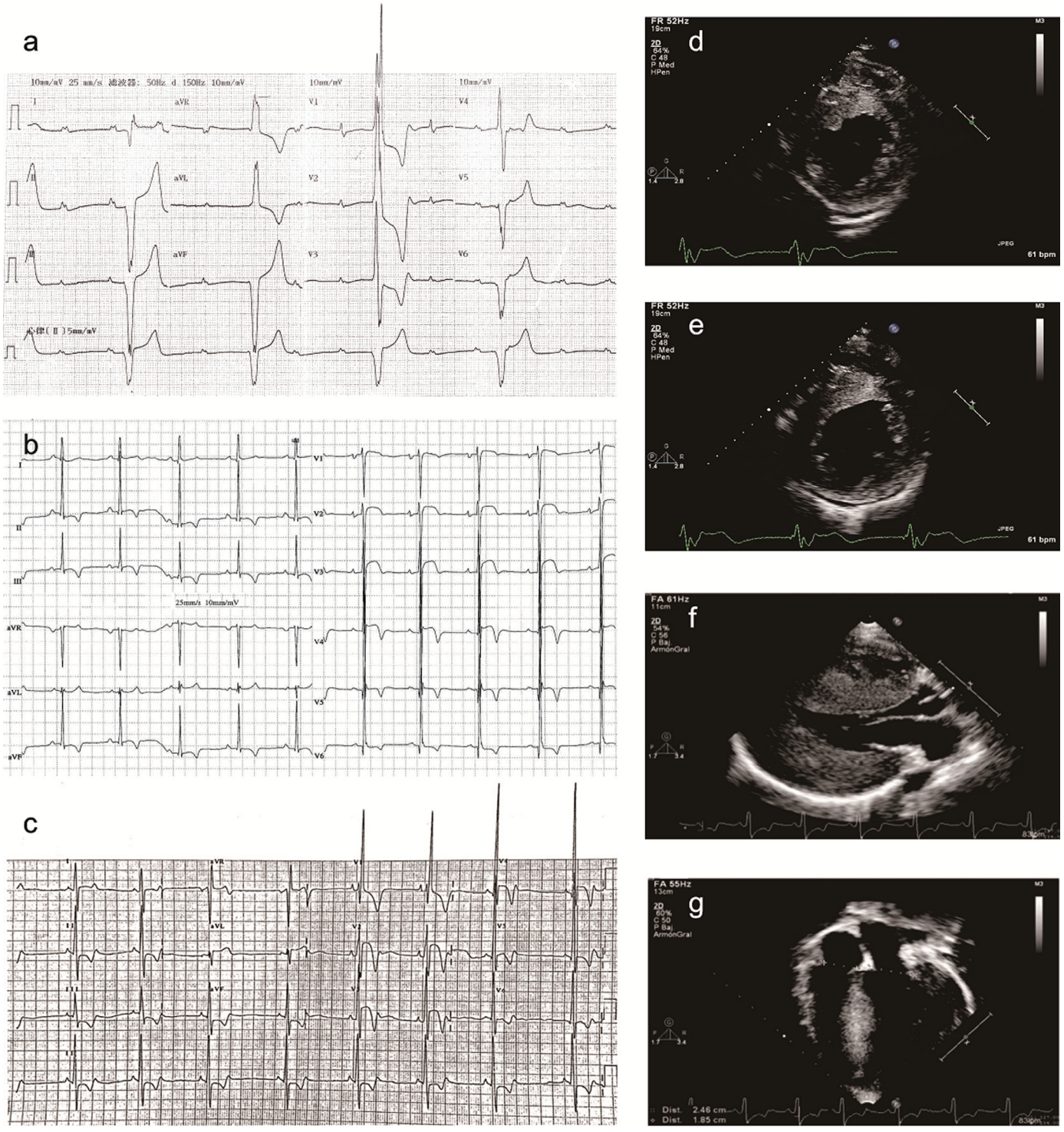

Fig. 2. Clinical records of novel *PRKAG2* mutation carriers. (**a-c**) 12-lead ECG of *PRKAG2*-R302P, L341S and H401D carrier at baseline (Proband 8–10). (**d-e**) Echo images of Proband 7 with R302P in a short axis view of chord and papillary muscle level of LV, showing increased thickness of LV. (**f-g**) Echo image of Proband 9 with H401D in a long axis view of the LV and a four chambers view, showing increased thickness of the interventricular septum and lateral wall of LV.

sodium channel protein (Nav1.5), which was mainly distributed in the cell membrane (Supplementary Fig. 9).

In addition to the typical cardiac phenotype of the *PRKAG2* syndrome, 50.0% of probands had associated hypertension, and 41.7% hyperlipidemia. The sister of Proband 4 with ventricular preexcitation, conduction disease, bradycardia, atrial fibrillation and septal thickness of 28 mm, developed acute glomerulonephritis at 15 y/o, and it evolved into uremia with chronic renal failure at 26 y/o. Major clinical findings are summarized in Table 1, and details were described in Supplementary Materials.

3.2. Mutational spectrum

In total, 5 heterozygous *PRKAG2* mutations were identified in 12 independent probands (25 patients, Fig. 3a). The recurrent mutation R302Q (c.905G>A), was found in 7 families (Families 1–7; 16 patients,

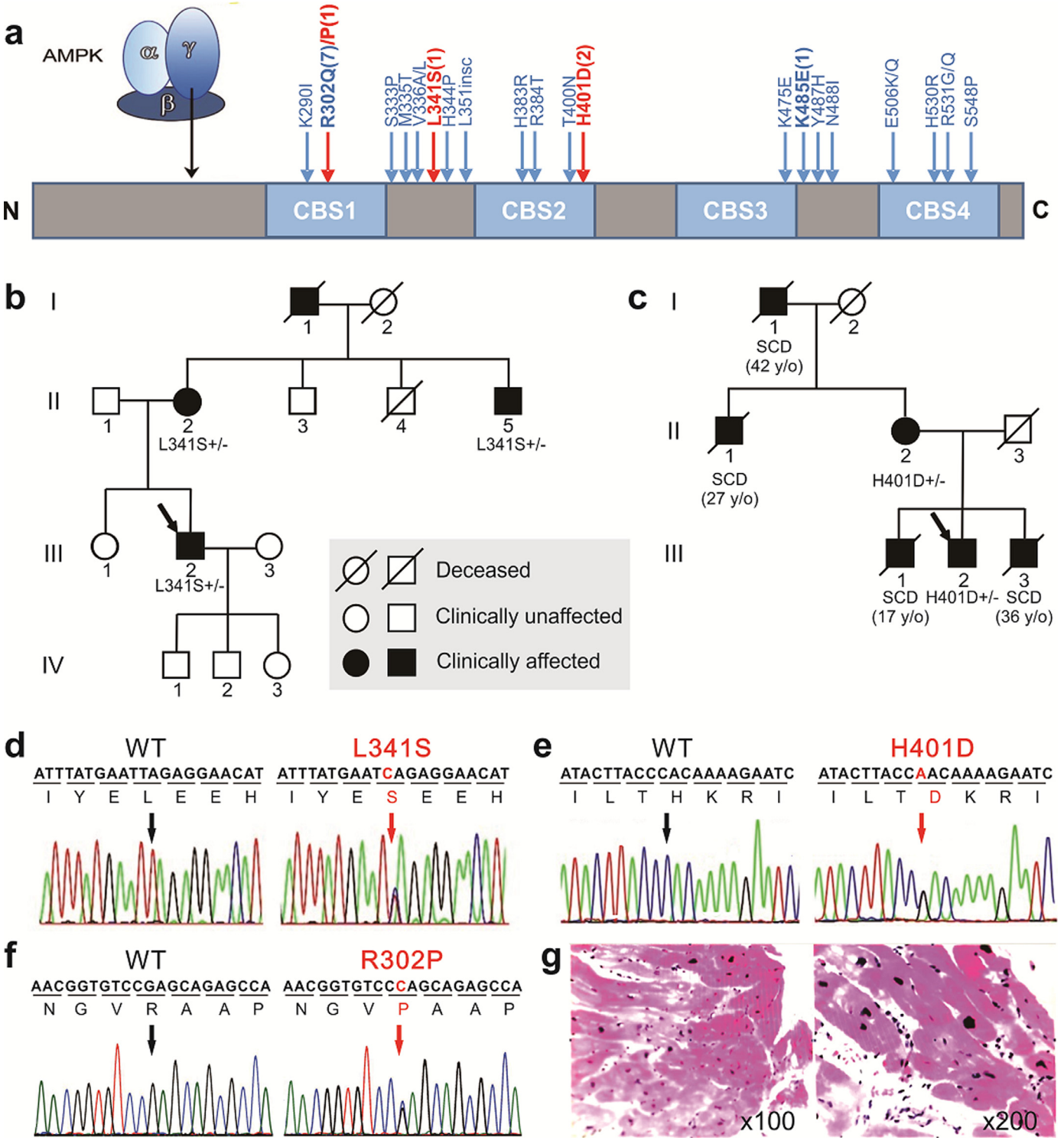

Fig. 3. Genetic information of novel mutations. (**a**) Schematic of AMPK γ2 subunit and *PRKAG2* mutations discovered thus far. Novel mutations are shown in red. (**b-c**) Pedigree of the *PRKAG2*-L341S and H401D mutation carriers (Proband 9&10). (**d-f**) DNA chromatogram of L341S, H401D and R302P. (**g**) Histopathology of ventricular sections with Congo-Red staining from proband 8. (For interpretation of the references to color in this figure legend, the reader is referred to the web version of this article.)

Fig. 1). Proband 7 also had a transition at c.905G>C that led to the novel mutation R302P (Fig. 3f). Genetic screening of Family 8 (3 cases, Fig. 3b) revealed a novel mutation consisting of a C-to-T transition at nucleotide 1022 (c.1022C>T), predicting a substitution of a serine for leucine at 341 (L341S, Fig. 3d). Screening of Family 9 (Fig. 3c) and 10 (3 cases) discovered another new mutation, H401D (c.1201C>G, Fig. 3e). These latter 3 variants have not been previously described in any publication or public databases, such as HGMD, dbSNP, NHLBI GO ESP and ClinVar, Gnomad, or in ExAC database. All were predicted to be possibly damaging by PolyPhen, damaging by SIFT, and deleterious by Provean; and changed the physico-chemical property of the reference amino acid (Grantham score). Supplementary Table 3 shows the predicted consequence of the mutations discovered in this study. The mutations were located in the first cystathionine beta-synthase (CBS) domain, the linker between the first and second CBS domain, and in the second CBS domain. These novel variants were located at residues highly conserved among species (Supplementary Table 2), showed co-segregation in all affected family members, and were absent in healthy

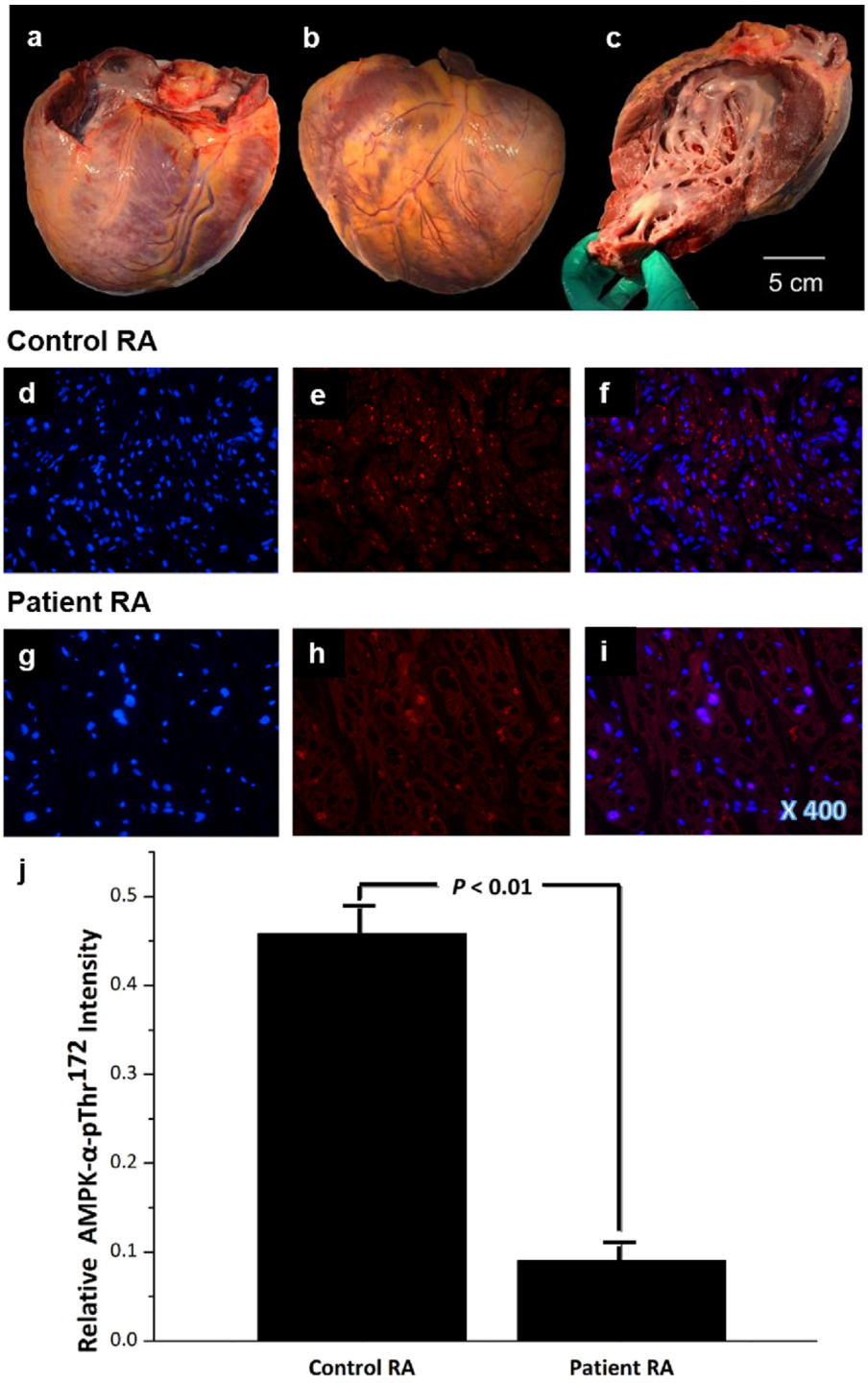

Fig. 4. The macroscopic image and AMPK quantification of the original heart from Proband 12. (**a-c**) The front/back/side view of the original heart. The apex is blunt, and the fat is slightly increased. The left ventricular wall is obviously thickened, and the subendocardial fibers are increased. (**d-i**): Phosphorylated AMPK of myocardial tissue (× 400 fold). In **d&g/e&h/f&i**, nucleuses/phosphorylated AMPK/the overlap are stained in blue/red/both. **j**: Quantification of phosphorylated AMPK (control myocardium: $n = 461$; patient myocardium: $n = 450$). (For interpretation of the references to color in this figure legend, the reader is referred to the web version of this article.)

family members. One *de novo* mutation, K485E (c.1453A>G), has been reported by our group previously (Family 12) [11].

3.3. Computational modeling prediction (See details in supplementary materials)

3.3.1. Structural comparison reveals the impact of ligands on domain conformation

In order to understand the regulatory behavior of AMPK in response to different ligands, we compared crystal structures of the kinase in complex with a variety of known binding ligands (Supplementary Fig. 10). Examination of the ligand-dependent root mean squared displacement (RMSD) revealed that R302 and K485 had strong conformational dependence on the bound ligand (Fig. 5a and b).

3.3.2. Electrostatic calculations suggest essential role of K485, R302

New electrostatic calculations reveal the carbonyl group introduced by the R302Q substitution leads to an increased region of negative charge around the sidechain (Fig. 6a and b). The carbonyl group in R302Q thus leads to repulsive interactions with the phosphate

Table 1
Characteristics of probands carrying *PRKAG2* mutation.

Proband No.	1	2	3	4	5	6	7	8	9	10	11	12	Summary (Average)
PRKAG2 mutation	R302Q (reported)	R302Q (reported)	R302Q (reported)	R302Q (reported)	R302Q (reported)	R302Q (reported)	R302Q (reported)	R302P (novel)	L341S (novel)	H401D (novel)	H401D (novel)	K485E (reported)	
Gender (M/F)	M	M	M	M	M	F	F	M	M	M	F	M	75.0%-M; 25.0%-F
Age at Dx (y/o)	27	15	30	16	15	40	27	24	15	14	26	15	(22.0 ± 8.3)
Symptom	chest distress, syncope, headache,	headache, chest distress, syncope	headache, chest distress, syncope	chest pain, syncope	palpitation, syncope	syncope	chest distress, palpitation	chest distress, palpitation, syncope	–	palpitation, dizziness, syncope	syncope	chest pain, chest distress, palpitation	91.7%-Sym: 8.3%-Asym
Biopsy	–	–	–	–	–	–	–	+	–	–	–	+	16.7%
Bradycardia (HRmin, bpm)	+ (24)	+ (51)	+ (40)	+ (28)	+(39)	+(30)	+ (44)	+ (25)	+ (25)	+ (49)	+ (45)	+ (35)	100% (36.3 ± 9.8)
CCD	III°AVB	complete LBBB	II° AVB (type 2)	III°AVB	III°AVB	III°AVB	III°AVB + complete LBBB	III°AVB	II° AVB (type 2)	pauses up to 3.0 s	2:1 heart block	II° AVB (type 2)	100%
Preexcitation	–	+	+	+	+	+	+	–	–	+	–	+	66.7%
Premature beat	–	+	–	+	–	–	+	+	–	+	–	+	50.0%
PSVT/AF	–	–	–	–	+	–	+	–	–	–	+	+	33.3%
SCD	–	–	–	–	–	–	+	–	–	+	–	–	16.7%
HCM	+	+	+	+	+	+	+	+	+	+	+	+	100%
NYHA	II	III	II	II	III	II	III	III	I	III	III	IV	III
EF (%)	59	76	57	60	30	45	67	42	57	69	64	40	(56.7%±13.5%)
Thickest Wall / Location (mm)	30/septal	36/septal	30/septal	44/septal	34/apical	19/septal	36/septal	18/septal	19/septal	33/septal	30/apical	32/septal	(31.2 ± 7.2)
HBP (mmHg)	–	–	–	–	–	+ (140/90)	–	+ (140/90)	+ (172/94)	+ (130/85)	+ (200/100)	+ (155/93)	50.0% (156.2 ± 26.0 / 92.0 ± 5.0)
Hyperlipidemia	–	–	–	–	+	+	+	+	–	–	+	–	41.7%
Biochemical Marker	↑cTnI, ↑CK-MB, ↑ALT, ↑GGT	↑cTnI, ↑CK-MB, ↑BNP	↑cTnI, ↑BNP	↑cTn, ↑cTnI, ↑BNP	–	–	↑LDH, ↑cTnI, ↑CK-MB	↑cTnI, ↑BNP	–	–	–	↑LDH	58.3%
Drug	metoprolol, benazepril	–	Diltiazem, amiodarone, nicorandil,	trimetazidine	metoprolol, captopril	coumadin, bisoprolol	Candasartan, Bisoprolol, ASA, lasix	metoprolol, spirolactone, Vasorel	Bisoprolol, Rosuvastatin, Benazepril, Furosemide, Spironolactone, Nicorandil	Coveram	metoprolol	Ramipril, Amlodipine, atorvastatin, Warfarin, Verapamil, Ramipril,	Rosuvastatin
metoprolol	91.7%												
Implantation	pacemaker	pacemaker	pacemaker	pacemaker	pacemaker	ICD	pacemaker	pacemaker	pacemaker	ICD	pacemaker	pacemaker	100%
Ablation	–	–	–	–	+ (failed)	–	–	–	–	–	–	+	16.7%
Septal myectomy	–	+ (die of complication at 25 y/o)	–	–	–	–	–	–	–	–	–	–	8.3%
Transplantation	–	–	–	–	–	–	–	–	–	–	–	+ (at 22 y/o)	8.3%
Family carriers	0	0	2	4	3	0	1	0	2	1	0	0 (*de novo*)	total 13
Family history of SCD (No)	+ (3)	+ (1)	–	+ (7)	+(1)	+(2)	–	–	–	–	+ (4)	–	50.0% (total 18, age 29.8 ± 11.4 y/o)
Family history of HF (No)	+ (1, died at 52 y/o)	+ (1, died at 44 y/o)	–	+ (2, died at 52, 54 y/o) transplantation) transplantation)	– – 41.7% (total 6)	– –	– + (1,	–	+ (1,				

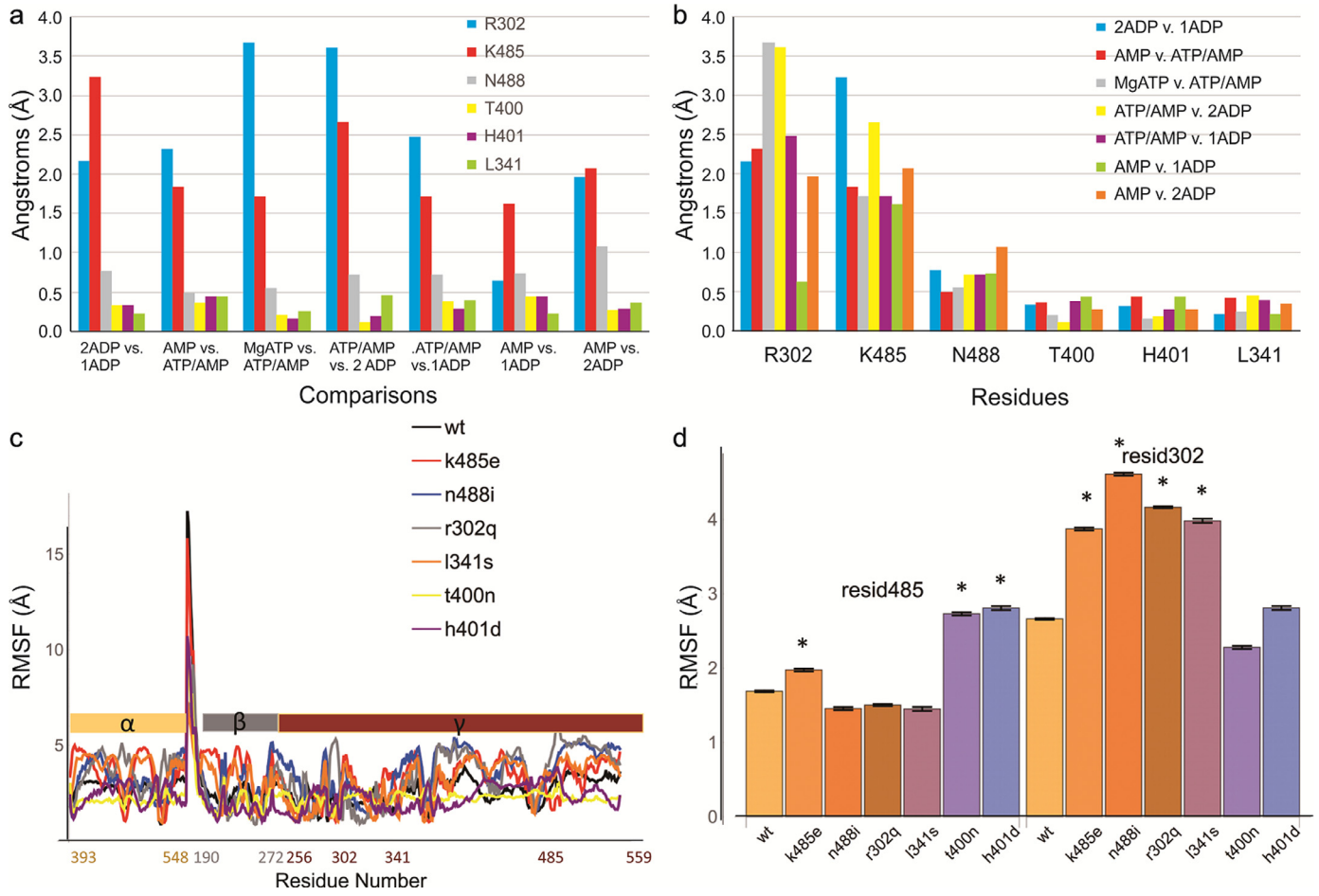

Fig. 5. RMSD comparison of AMPK grouped by (**a**) residue location and (**b**) ligand identity. Structures were aligned on the gamma subunit prior to all RMSD calculations. (**c**) RMSF plots for the seven simulated variants. (**d**) RMSF values for the mutated residues at positions 485 and 302; the simulations from which the data were obtained are shown along the x-axis. Values with significant difference from the WT are indicated with an asterisk (see details of p-value at Supplementary Table 4).

group(s) on incoming ligands and a consequent decrease in ligand binding ability. Residues N488 and L341 were found in helical domains that flank the critical salt bridge formed by K485 (Fig. 6c, Supplementary Fig. 10). Both N488I and L341S involved substitution between hydrophilic and hydrophobic residues, which would lead to significant structural rearrangement. Electrostatic calculations on L341S revealed serine substitution for leucine increases the polarity of this region of the helix, and introduces a new area of negative charge around L341 (Fig. 6d). These results were consistent with a 50% decrease in the (helical) secondary structure of this region shown in our simulations of N488I and L341S. Residues T400N and H401D were found adjacent to the nucleotide binding region in CBS-2 domain. The H401D mutation removed a significant area of positive charge in the nucleotide binding pocket, replacing it with the negatively-charged aspartate sidechain (Fig. 6e).

3.3.3. All mutants show coupling between nucleotide binding site and regulatory salt bridge

While the R302Q/P mutant, occurring in the nucleotide binding pocket, was expected to display elevated fluctuations, we were surprised to observe that almost all mutations resulted in a significant increase in the mobility of R302 (Fig. 5d, Supplementary Table 4). These data indicated even remote mutations on the surface of the protein (such as N488I and L341S) can lead to a disruption in the nucleotide binding pocket and a consequent decrease in binding affinity for ligands. Interestingly, H401D and T400N disrupted both the nucleotide binding pocket and the inter-subunit interface. While H401D did not directly change the mobility of R302 (Fig. 5d), H401D generated a strong local negative charge, that flipped H530 and attracted R531, pulling them both away from the nucleotide binding pocket and thus disorienting the nucleotide binding site in the Bateman domain (Fig. 6f and g).

3.3.4. Analysis of fluctuations demonstrates long-range effect of mutations

The RMSF spike at position 103 (Fig. 7c) was due to a break in the protein backbone where significant mobility was observed at the end of each chain. All mutants showed significantly greater RMSF (two-fold increase) and significantly lower secondary structure (five-fold decrease in N488I, ten-fold decrease in K485E) in the N-terminal region, indicating the significant and drastic structural effect of the mutants on the regulatory domain. They also showed significantly greater fluctuations in the CBS domains, suggesting these mutations lead to a systematic disruption of the ligand binding interfaces. The notable exception to this was the region around K485, the region involved in the regulatory salt bridge interface with the beta chain (Fig. 5c).

3.3.5. Transfer entropy identifies pathways of communication stemming from CBS-4

Following the approach of Hacisuleyman [10], we reported the entropy generated by each residue of AMPK (Fig. 7a). The strongest driving behavior was observed from residues at the beginning of the beta subunit, known as the alpha-gamma subunit binding sequence

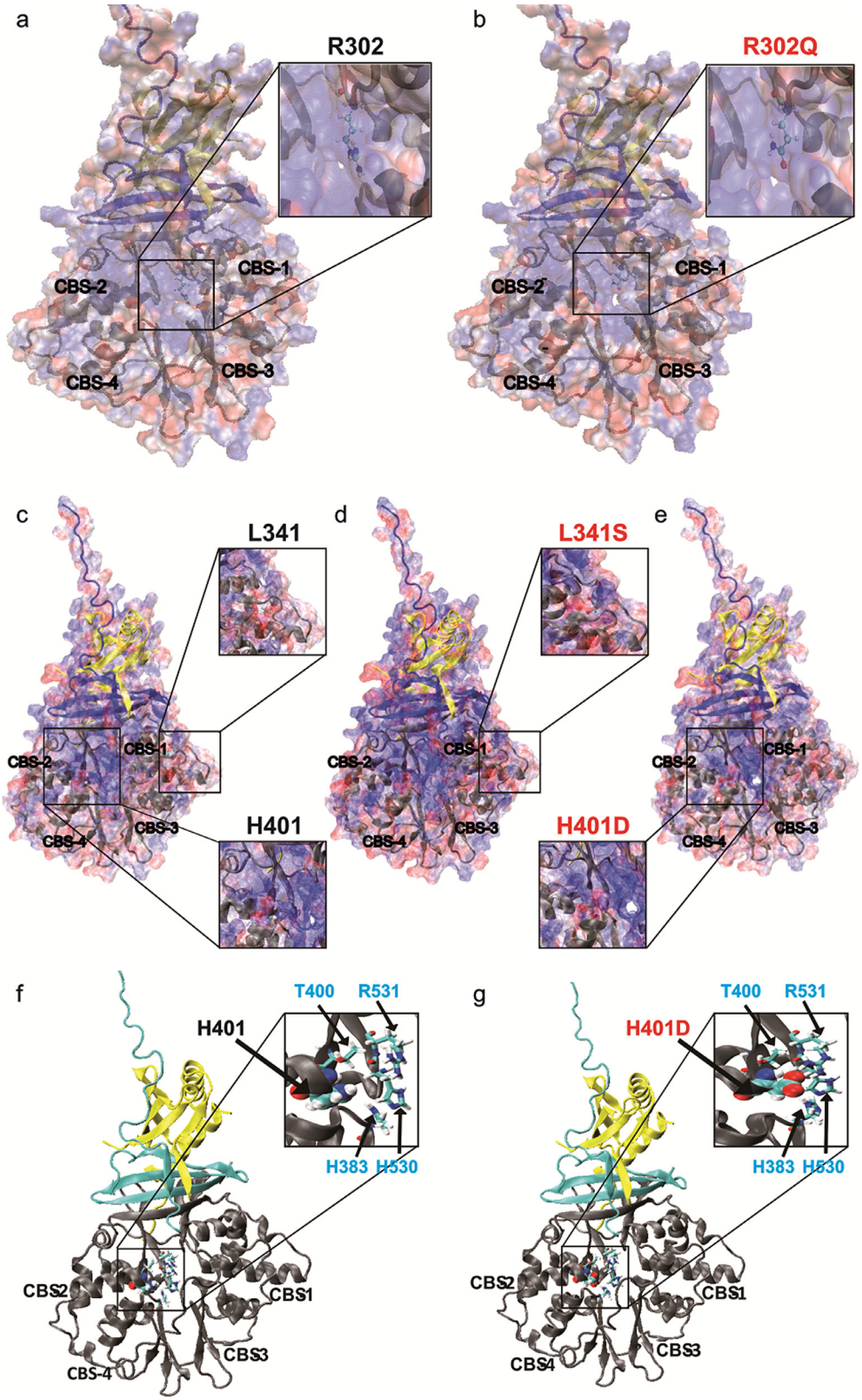

Fig. 6. Electrostatic surfaces of different mutations compared with WT. (**a&b**) AMPK-WT *vs.* R302Q. (**c-e**) AMPK-WT *vs.* L341S and H401D. Change in the orientation of the nucleotide binding pocket in H401 (**f**) induced by the H401D mutation (**g**). Positively/negatively-charged regions are shown in red/blue. (For interpretation of the references to color in this figure legend, the reader is referred to the web version of this article.)

(SBS). Fig. 7b–e provides a plot of the row of the transfer entropy matrix corresponding to residues R302, K485, H401, and L341. K485 and H401 appeared to provide approximately equal entropy out to the beta subunit as well as to the CBS-3 and CBS-4 sites. R302 and L341 provided a relatively larger entropy out to the SBS domain for communication, and these residues also provided higher entropy out

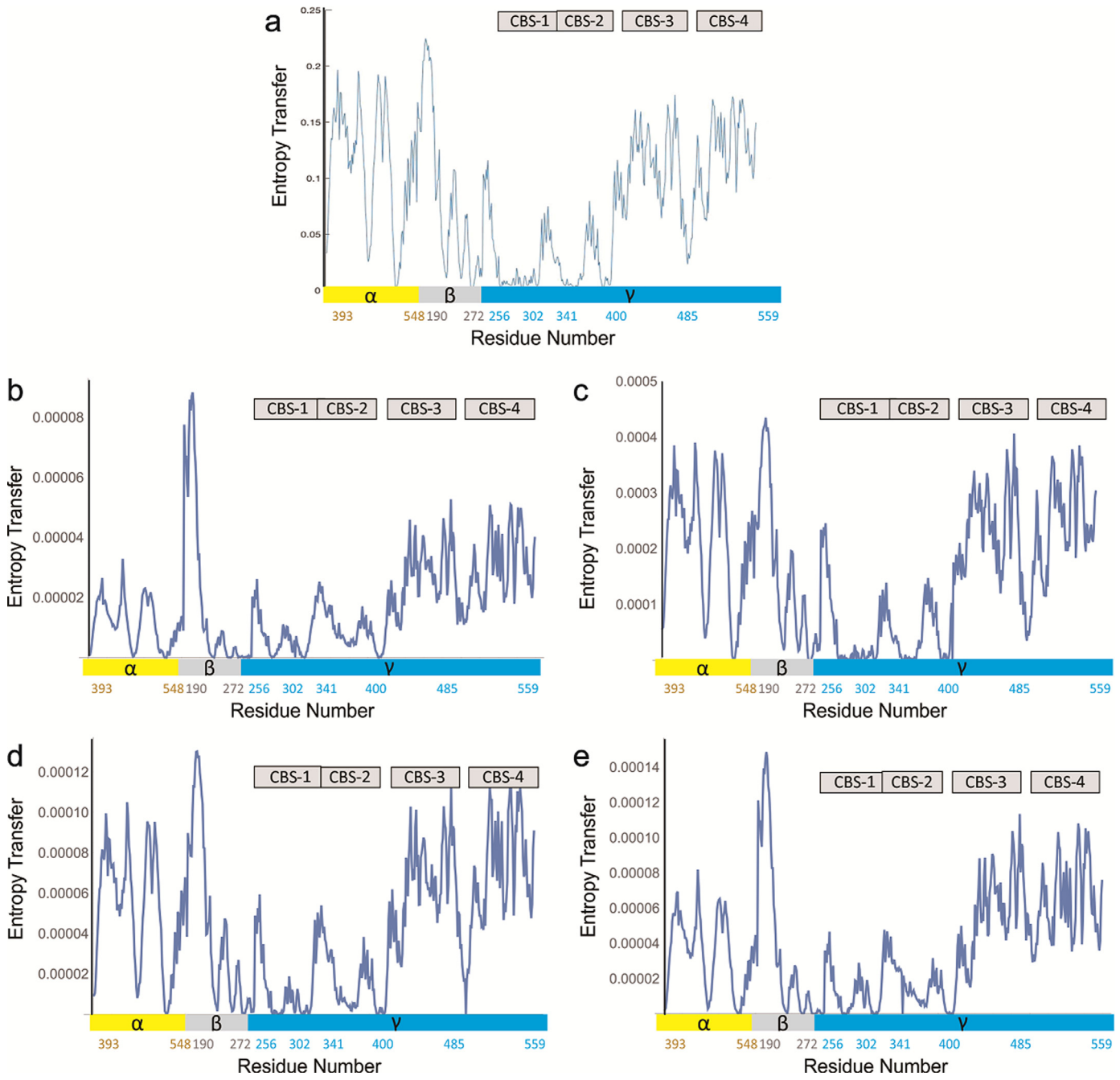

Fig. 7. Entropy transfer from each residue (**a**), and from R302 (**b**), K485 (**c**), H401 (**d**), and L341 (**e**) to the rest of the protein.

to K485 than the other residues, or than the protein as a whole, indicating again the plausible pathway, by which binding information was communicated from the CBS domains through R302 *via* the K485/D248 salt bridge to the SBS domain and ultimately to the catalytic domain of δ subunit.

4. Discussion

In the present study, 5 *PRKAG2* mutations in 12 families with typical phenotypes are identified, which include LVH, CCD, sinus node dysfunction, ventricular pre-excitation, atrial tachyarrhythmia, cardiomyocyte glycogen excess, and propensity to SCD or HF (Fig. 8). The latter may require heart transplantation in time. The probands bearing a *PRKAG2* mutation present typically with palpitations, syncope, chest pain, or features of HF. Only 1 is identified after an abnormal ECG (Proband 7). While penetrance is 100%, as prescribed previously [14], the disease progression in our objectives for the same mutation have interfamilial variability, even heterogeneity, *i.e.* Family 4. The overall mean age at diagnosis is around 30 y/o for all reported mutations, 19 y/o for N488I, and 36 y/o for R302Q [15]. Pediatric or even antenatal presentations have been reported for some variants, including H383R, R384T, R531G, and R531Q [3,16,17], and linked to a more severe clinical phenotype. The present *PRKAG2* cohort is identified much earlier (~20y/o), which is partly due to malignant manifestation at a young age in some cases, timely genetic screening, and family consultation.

LVH represents the most common clinical features in patients with *PRKAG2* mutations [14]. The youngest carrier in our cohort with LVH is 7 years old. In general, LVH may be concentric or, preferentially involve the septum, while asymmetric hypertrophy could also involve the mid-inferolateral LV [18]. This study is the first to

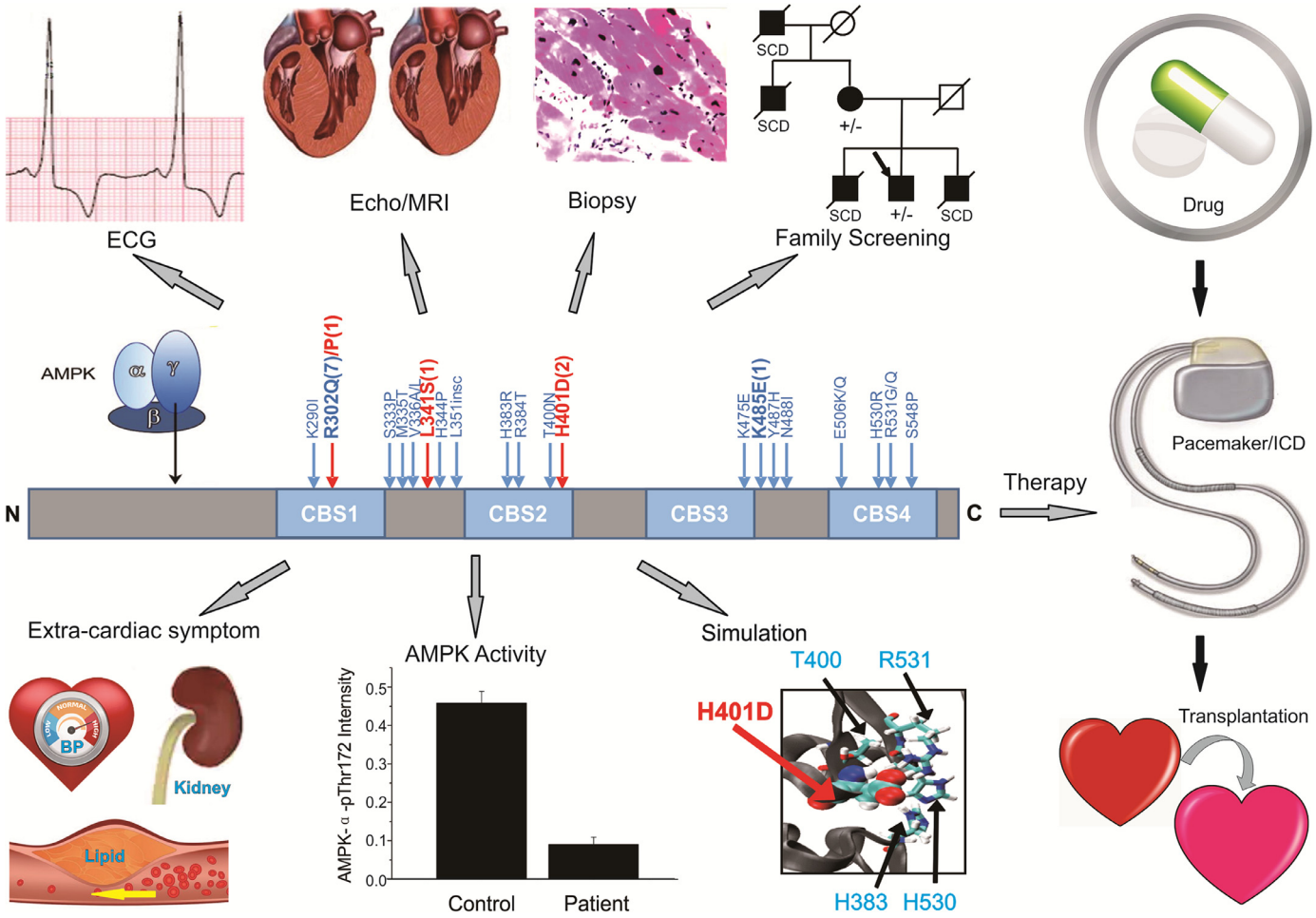

Fig. 8. Unique genetic background, clinical manifestation and underlying mechanisms, as well as management options of *PRKAG2* cardiac syndrome. ECG, electrocardiogram; MRI, magnetic resonance imaging; Echo, echocardiogram; ICD, implantable cardioverter-defibrillator.

describe evidence of apical hypertrophy in *PRKAG2* syndrome patients. Whether this phenomenon represents the impact of epigenetic, genetic, or environmental modifiers is unclear.

Recent published summaries estimate SCD to affect 9–20% of mutation carriers, with a mean age of death at 33–44 years [15,19]. Given the high rate of pacemaker implantation (reported as ~43% [15]), it is probable that timely pacemaker implantation prevents SCD in many mutation carriers. Although a pacemaker may improve the life span of most patients, patients may progress to severe HF and require transplant. In our cohort, Patient III3 in family 6 (without genotyping) suffered from SCD after implantation of pacemaker; while patient II5 in family 9 with L341S (Fig. 3B) and the Proband 12 with K485E (Fig. 4A–C) received cardiac transplantation on time due to prompt genetic screening, functional prediction and adjusted clinical management.

One should note that systolic HF appears to be frequent in the setting of a *PRKAG2* mutation, being reported in the former study in ~12% of all patients [15] and even up to 25% in certain cohorts [19]. Previously published mutations related to HF or heart transplantation are V336A, R350_E351insL, H383R, H530R, and R531Q [17,19,20]. In contrast, the frequency appears lower with the two most frequent mutations (R302Q and N488I), with transplantation reported in only one [3]. Here, we add an additional 2 mutations - carriers with L341S and K485E received transplantation (9.1%) at relatively young ages. Unexpectedly, in 7 R302Q mutant families, 4 clinically affected cases died from HF, including one with a pacemaker for nearly 30 years. Meanwhile, a profound elevation in plasma N-terminal pro-BNP was detected in 3 probands with R302Q and 1 with R302P, which is in accordance with observations from studied mouse models [5,21]. Similar clinical observation is only reported in one E506K carrier [22].

Although extracardiac manifestations have not previously been emphasized, we observed more than half of our probands to have elevated blood pressure at young ages. It was observed that *PRKAG2* mutant mice (equivalent to human with R302Q) with chronic AMPK activation exhibit metabolism changes [23]. Four of our 7 index cases bearing the R302Q manifest a congruent phenotype, such as hyperphagia and obesity/overweight (BMI>24). Three affected patients had reported dyslipidemias. In mouse models, TG^{R302Q} mice, but not TG^{N488I} mice, exhibited severe kidney injury characterized by glycogen accumulation, inflammation, apoptosis, cyst formation, and impaired renal function after a high-fat diet [24]. Among our 25 cases, one R302Q patient was observed with renal failure, raising the possibility of direct association with this predominant cardiac phenotype, as indicated by a recent GWAS and case report [25]. Although uncertainty remains of a direct link to *PRKAG2* disease, one may speculate that perturbed AMPK related signaling in vascular endothelial cells, smooth muscle cells, pancreatic islet, renal function, and/or 3-Hydroxy-3-Methylglutaryl-CoA Reductase (HMGCR) could provoke these extracardiac issues [26–28]. *PRKAG2* syndrome is thought to frequently be accompanied by chronotropic incompetence [3,15]. Animal study from Yavari and Ashrafian suggests that AMPK functions in an organ-specific manner to maintain cardiac energy homeostasis and determines cardiac physiological adaptation to exercise by modulating intrinsic sinoatrial cell via sarcolemmal hyperpolarization-activated current (I_f) and ryanodine receptor-derived diastolic local subsarcolemmal Ca^{2+} release [29]. The key step in the management of

PRKAG2 syndrome is its prompt identification in cases of unexplained familial LVH. The identification of an isolated short PR interval and/or preexcitation on ECG is a strong diagnostic indication. Ultimately, genotyping is required for a definitive diagnosis [15], positive genetic identification enables cascade screening of at-risk family members.

Although the *PRKAG2* mutations result in similar phenotypes, the influences on cardiac AMPK activity are distinct [5,21], which indicates that the molecular linkage between AMPK activity and the syndrome is still obscure and requires further investigation. Here, we first observed a significantly reduced AMPK activity in human heart with K485E. The underlying mechanism may be that glycogen accumulation leads to negative feedback of AMPK activity. Prominent myofibril destruction is the possible cause of early HF in patients with K485E mutation.

In 1995, a single disease locus for an inherited form of ventricular pre-excitation and HCM was mapped to chromosome 7q3. In 2001, Gollob et al. linked a large Canadian family with ventricular preexciation, conduction disease, atrial arrhythmias and LVH to the same genetic locus and first described mutations in *PRKAG2* as a cause of this unique syndrome [3,30]. Subsequent mouse modelling of the described R302Q mutation confirmed the pathological basis of cardiac disease to be related to excessive cardiac glyogenosis [5]. Since the identification of *PRKAG2* as a cause of this condition, only around 200 patients have been reported in the literature. Of these cases, 22 distinct heterozygous variants have been described and all of them are located with, or in close proximity to, the adenine nucleotide binding CBS domains (Fig. 3A), which are recognized as functional regions interacting with AMP, ADP or ATP. The most frequently identified mutations are R302Q (135 cases from 14 families, ~57%), followed by N488I (40 cases from 2 families, ~21%) [15]. This study has added 22 more *PRKAG2* cases and 4 novel mutations in the exploration journey of the disease.

All mutants here lead to disruption of the ligand-binding interfaces and/or break communication with the alpha and beta subunits which directly impacts the catalytic portion of the kinase. R302 provides an important electrostatic interaction to direct ligand binding in the regulatory subunit; mutation of this residue results in increased mobility of the arginine and disruption of the essential positively-charged pocket required for binding the phosphate group(s) on incoming ligands. The importance of R302 is highlighted further by the N488I and L341S mutations, since both could result in destabilization of R302. Thus, while L341 does not play a direct role in ligand binding, mutation at this residue directly influences it. Communication between the subunits is facilitated by a salt bridge between D248 and K485 in the beta and gamma subunits, respectively. Interestingly, even in the mutants, this region shows the lowest dynamic fluctuation, indicating the critical nature of this interface. Mutations in this domain are consequently pathological, as evidenced not only by the direct breaking of the salt bridge with K485E, but also by the pathological effect of disrupting the secondary structure of the region (N488I and L341S). Thus, we predict with confidence the role of the neighboring Y487H, as the disruption in the secondary structure of this region has been shown to lead to a loss of both ligand binding affinity and regulatory communication mediated by the K485-D248 salt bridge. T400 and H401 provide stabilizing interactions that orient the nucleotide binding pocket. Mutations of these residues both disrupt the nucleotide binding interface and destabilize the salt bridge. Recently, three-dimensional modelling of H401Q shows similar functional consequences [31].

Finally, a comprehensive picture of the pathways for communication in the kinase and the role of the CBS-4 domain as the AMP-binding site are provided, which facilitates and directs the other binding sites, including CBS-3, as well as R302, T400 and H401. It shows that K485 plays an intermediate role in facilitating communication between the binding sites and the catalytic domain. We propose a pathway for communication connecting R302 and H401 to L341 and K485, which in turn pass information to the SBS domain of the beta subunit to be relayed to the alpha subunit.

5. Limitation and conclusion

Among 885 subjects with HCM, we found 12 with *PRKAG2* mutations (1.4%). This is probably an underestimation of *PRKAG2* incidence because some patients may not present as hypertrophy. Another limitation is that EMB has been used as part of the investigative workup in only 2 cases showing aggressive phenotypes, so their results cannot be applied to all *PRKAG2* cases. However, given its attendant risks, current guidelines recommend EMB to be considered in a minority of cases where noninvasive assessment has failed to reveal the cause [32]. Although we have done our best, 21 members are still lost due to various reasons without molecular biopsy. This reminds us that the diagnosis and treatment of *PRKAG2* syndrome are a systematic social behavior and require more attention. We do realize that some researchers reported a very high incidence of a variant of preexcitation, fasciculoventricular pathway mainly, as the substrate for preexcitation in *PRKAG2* carriers [33]. Unfortunately, we cannot identify the prevalence of fasciculoventricular pathway in our *PRKAG2* cohort. We could not make an analysis on VT/VF incidence, since differential diagnosis from pre-excited AT-AF could not be made. Although applying the results from preclinical experiment into patients, and benefitting them are not achievable in the short term, those studies and the present investigation hold promise not only to understanding the cellular energy sensor and the potential target to treat more prevalent metabolic and cardiac diseases, but also to seeking specific therapeutics for *PRKAG2* syndrome.

Declaration of Competing Interest

The authors report no relationships that could be construed as a conflict of interest.

Acknowledgment

We gratefully acknowledge productive conversations with and contributions from Theresa Schmitz, and Luisa Garcia-Michel. We also appreciate assistance by Dr. Yan Huang for making the figures.

Funding

The current work was supported by the National Natural Science Foundation Project of China (Grant Nos. 81201552, 81671693 and 81670304); the International Science and Technology Cooperation Program of China (2014DFA31980); Distinguished Professor of Chutian scholar program of Hubei province, Shanxi Provincial Key Project (2017ZDXM-SF-058); Key Science and Technology Innovation Team Project of Shanxi Province (2014KCT-20); National Institutes of Health of USA (NIH R56 [HL47678] and NIH R01 [HL138103]).

Supplementary materials

Supplementary material associated with this article can be found in the online version at doi:10.1016/j.ebiom.2020.102723.

References

[1] Gersh BJ, Maron BJ, Bonow RO, Dearani JA, Fifer MA, Link MS, et al. 2011 ACCF/AHA guideline for the diagnosis and treatment of hypertrophic cardiomyopathy: a report of the American college of cardiology foundation/American heart association task force on practice guidelines. Circulation 2011;124(24):e783–831.

[2] Authors/Task Force m, Elliott PM, Anastasakis A, Borger MA, Borggrefe M, Cecchi F, et al. 2014 ESC guidelines on diagnosis and management of hypertrophic cardiomyopathy: the task force for the diagnosis and management of hypertrophic cardiomyopathy of the european society of cardiology (ESC). Eur Heart J 2014;35(39):2733–79.

[3] Gollob MH, Seger JJ, Gollob TN, Tapscott T, Gonzales O, Bachinski L, et al. Novel PRKAG2 mutation responsible for the genetic syndrome of ventricular preexcitation and conduction system disease with childhood onset and absence of cardiac hypertrophy. Circulation 2001;104(25):3030–3.
[4] Gollob MH, Roberts R. AMP-activated protein kinase and familial Wolff-Parkinson-White syndrome: new perspectives on heart development and arrhythmogenesis. Eur Heart J 2002;23(9):679–81.
[5] Sidhu JS, Rajawat YS, Rami TG, Gollob MH, Wang Z, Yuan R, et al. Transgenic mouse model of ventricular preexcitation and atrioventricular reentrant tachycardia induced by an AMP-activated protein kinase loss-of-function mutation responsible for wolff-parkinson-white syndrome. Circulation 2005;111(1):21–9.
[6] Xie C, Zhang YP, Song L, Luo J, Qi W, Hu J, et al. Genome editing with CRISPR/Cas9 in postnatal mice corrects PRKAG2 cardiac syndrome. Cell Res 2016;26(10):1099–111.
[7] Yavari A, Sarma D, Sternick EB. Human gamma2-AMPK mutations. Methods Mol Biol 2018;1732:581–619.
[8] Zhan Y, Sun X, Li B, Cai H, Xu C, Liang Q, et al. Establishment of a PRKAG2 cardiac syndrome disease model and mechanism study using human induced pluripotent stem cells. J Mol Cell Cardiol 2018;117:49–61.
[9] Hinson JT, Chopra A, Lowe A, Sheng CC, Gupta RM, Kuppusamy R, et al. Integrative analysis of PRKAG2 cardiomyopathy iPS and microtissue models identifies ampk as a regulator of metabolism, survival, and fibrosis. Cell Rep 2016;17(12):3292–304.
[10] Hacisuleyman A, Erman B. Causality, transfer entropy, and allosteric communication landscapes in proteins with harmonic interactions. Proteins 2017;85(6):1056–64.
[11] Liu Y, Bai R, Wang L, Zhang C, Zhao R, Wan D, et al. Identification of a novel de novo mutation associated with PRKAG2 cardiac syndrome and early onset of heart failure. PLoS One 2013;8(5):e64603.
[12] Arad M, Benson DW, Perez-Atayde AR, McKenna WJ, Sparks EA, Kanter RJ, et al. Constitutively active amp kinase mutations cause glycogen storage disease mimicking hypertrophic cardiomyopathy. J Clin Invest 2002;109(3):357–62.
[13] Back Sternick E, de Almeida Araujo S, Ribeiro da Silva Camargos E, Brasileiro Filho G. Atrial pathology findings in a patient with PRKAG2 cardiomyopathy and persistent atrial fibrillation. Circ Arrhythm Electrophysiol 2016;9(12).
[14] Murphy RT, Mogensen J, McGarry K, Bahl A, Evans A, Osman E, et al. Adenosine monophosphate-activated protein kinase disease mimicks hypertrophic cardiomyopathy and Wolff-Parkinson-White syndrome: natural history. J Am Coll Cardiol 2005;45(6):922–30.
[15] Porto AG, Brun F, Severini GM, Losurdo P, Fabris E, Taylor MRG, et al. Clinical spectrum of PRKAG2 syndrome. Circ Arrhythm Electrophysiol 2016;9(1):e003121.
[16] Akman HO, Sampayo JN, Ross FA, Scott JW, Wilson G, Benson L, et al. Fatal infantile cardiac glycogenosis with phosphorylase kinase deficiency and a mutation in the gamma2-subunit of AMP-activated protein kinase. Pediatr Res 2007;62(4):499–504.
[17] Burwinkel B, Scott JW, Buhrer C, van Landeghem FK, Cox GF, Wilson CJ, et al. Fatal congenital heart glycogenosis caused by a recurrent activating R531Q mutation in the gamma 2-subunit of AMP-activated protein kinase (PRKAG2), not by phosphorylase kinase deficiency. Am J Hum Genet 2005;76(6):1034–49.
[18] Poyhonen P, Hiippala A, Ollila L, Kaasalainen T, Hanninen H, Helio T, et al. Cardiovascular magnetic resonance findings in patients with PRKAG2 gene mutations. J Cardiovasc Magn Reson 2015;17:89.
[19] Thevenon J, Laurent G, Ader F, Laforet P, Klug D, Duva Pentiah A, et al. High prevalence of arrhythmic and myocardial complications in patients with cardiac glycogenosis due to PRKAG2 mutations. Europace 2017;19(4):651–9.
[20] Morita H, Rehm HL, Menesses A, McDonough B, Roberts AE, Kucherlapati R, et al. Shared genetic causes of cardiac hypertrophy in children and adults. N Engl J Med 2008;358(18):1899–908.
[21] Banerjee SK, McGaffin KR, Huang XN, Ahmad F. Activation of cardiac hypertrophic signaling pathways in a transgenic mouse with the human PRKAG2 thr400asn mutation. Biochim Biophys Acta 2010;1802(2):284–91.
[22] Bayrak F, Komurcu-Bayrak E, Mutlu B, Kahveci G, Basaran Y, Erginel-Unaltuna N. Ventricular pre-excitation and cardiac hypertrophy mimicking hypertrophic cardiomyopathy in a Turkish family with a novel PRKAG2 mutation. Eur J Heart Fail 2006;8(7):712–5.
[23] Yavari A, Stocker CJ, Ghaffari S, Wargent ET, Steeples V, Czibik G, et al. Chronic activation of gamma2 AMPK induces obesity and reduces beta cell function. Cell Metab 2016;23(5):821–36.
[24] Yang X, Mudgett J, Bou-About G, Champy MF, Jacobs H, Monassier L, et al. Physiological expression of AMPKgamma2RG mutation causes Wolff-Parkinson-White syndrome and induces kidney injury in mice. J Biol Chem 2016;291(45):23428–39.
[25] Giudici MC, Ahmad F, Holanda DG. Patient with a PRKAG2 mutation who developed immunoglobulin a nephropathy: a case report. Eur Heart J Case Rep 2019;3(2).
[26] Bonora M, Wieckowsk MR, Chinopoulos C, Kepp O, Kroemer G, Galluzzi L, et al. Molecular mechanisms of cell death: central implication of ATP synthase in mitochondrial permeability transition. Oncogene 2015;34(12):1608.
[27] Kottgen A, Pattaro C, Boger CA, Fuchsberger C, Olden M, Glazer NL, et al. New loci associated with kidney function and chronic kidney disease. Nat Genet 2010;42(5):376–84.
[28] Barnes BR, Marklund S, Steiler TL, Walter M, Hjalm G, Amarger V, et al. The 5′-AMP-activated protein kinase gamma3 isoform has a key role in carbohydrate and lipid metabolism in glycolytic skeletal muscle. J Biol Chem 2004;279(37):38441–7.
[29] Yavari A, Bellahcene M, Bucchi A, Sirenko S, Pinter K, Herring N, et al. Mammalian gamma2 AMPK regulates intrinsic heart rate. Nat Commun 2017;8(1):1258.
[30] Gollob MH, Green MS, Tang AS, Gollob T, Karibe A, Ali Hassan AS, et al. Identification of a gene responsible for familial Wolff-Parkinson-White syndrome. N Engl J Med 2001;344(24):1823–31.
[31] Albernaz Siqueira MH, Honorato-Sampaio K, Dias GM, Wilson JR, Yavari A, Filho GB, et al. Sudden death associated with a novel H401Q PRKAG2 mutation. Europace 2020:3076–93. doi: 10.1093/europace/euaa0014.
[32] Cooper LT, Baughman KL, Feldman AM, Frustaci A, Jessup M, Kuhl U, et al. The role of endomyocardial biopsy in the management of cardiovascular disease: a scientific statement from the American heart association, the American college of cardiology, and the european society of cardiology endorsed by the heart failure society of America and the heart failure association of the european society of cardiology. Eur Heart J 2007;28(24):3076–93.
[33] Sternick EB, Oliva A, Gerken LM, Magalhaes L, Scarpelli R, Correia FS, et al. Clinical, electrocardiographic, and electrophysiologic characteristics of patients with a fasciculoventricular pathway: the role of PRKAG2 mutation. Heart Rhythm 2011;8(1):58–64.